Autoreactive napsin A-specific T cells are enriched in lung tumors and inflammatory lung lesions during immune checkpoint blockade

Berner, F.; Bomze, D.; Lichtensteiger, C.; Walter, V.; Niederer, R.; Ali, O.H.; ... ; Flatz, L.

TUMOR IMMUNOLOGY

Autoreactive napsin A–specific T cells are enriched in lung tumors and inflammatory lung lesions during immune checkpoint blockade

Fiamma Berner[1]†, David Bomze[1,2,3]†, Christa Lichtensteiger[1], Vincent Walter[4], Rebekka Niederer[1,5], Omar Hasan Ali[1,6,7], Nina Wyss[1,5], Jens Bauer[8,9,10], Lena Katharina Freudenmann[9,11], Ana Marcu[9], Eva-Maria Wolfschmitt[9], Sebastian Haen[9]‡, Thorben Gross[9], Marie-Therese Abdou[1], Stefan Diem[12], Stella Knöpfli[1], Tobias Sinnberg[4,10], Kathrin Hofmeister[4], Hung-Wei Cheng[1], Marieta Toma[13], Niklas Klümper[14,15], Mette-Triin Purde[1], Oltin Tiberiu Pop[1], Ann-Kristin Jochum[1,16], Steve Pascolo[7], Markus Joerger[12], Martin Früh[12,17], Wolfram Jochum[16], Hans-Georg Rammensee[9,10,11], Heinz Läubli[18], Michael Hölzel[15], Jacques Neefjes[19], Juliane Walz[8,9,10,11,20], Lukas Flatz[1,4,5,7,12]*

Cancer treatment with immune checkpoint blockade (ICB) often induces immune-related adverse events (irAEs). We hypothesized that proteins coexpressed in tumors and normal cells could be antigenic targets in irAEs and herein described DITAS (discovery of tumor-associated self-antigens) for their identification. DITAS computed transcriptional similarity between lung tumors and healthy lung tissue based on single-sample gene set enrichment analysis. This identified 10 lung tissue–specific genes highly expressed in the lung tumors. Computational analysis was combined with functional T cell assays and single-cell RNA sequencing of the antigen-specific T cells to validate the lung tumor self-antigens. In patients with non–small cell lung cancer (NSCLC) treated with ICB, napsin A was a self-antigen that elicited strong CD8$^+$ T cell responses, with ICB responders harboring higher frequencies of these CD8$^+$ T cells compared with nonresponders. Human leukocyte antigen (HLA) class I ligands derived from napsin A were present in human lung tumors and in nontumor lung tissues, and napsin A tetramers confirmed the presence of napsin A–specific CD8$^+$ T cells in blood and tumors of patients with NSCLC. Napsin A–specific T cell clonotypes were enriched in lung tumors and ICB-induced inflammatory lung lesions and could kill immortalized HLA-matched NSCLC cells ex vivo. Single-cell RNA sequencing revealed that these T cell clonotypes expressed proinflammatory cytokines and cytotoxic markers. Thus, DITAS successfully identified self-antigens, including napsin A, that likely mediate effective antitumor T cell responses in NSCLC and may simultaneously underpin lung irAEs.

INTRODUCTION

Immune checkpoint blockade (ICB) therapy has revolutionized cancer treatment. These monoclonal antibodies diminish the inhibitory effect of molecules within the immune synapse, such as programmed cell death protein 1 (PD-1) or its ligand (PD-L1) and cytotoxic lymphocyte antigen-4 (CTLA-4), resulting in enhanced activation of T cells. ICB has significantly improved the survival of patients with cancer and has been approved for treating a variety of cancer types (*1*–*5*). However, reinvigoration of the immune system can result in severe autoimmune toxicities that are known as immune-related adverse events (irAEs). The incidence of irAEs depends on the class of ICB: irAEs occur in 72% of patients treated with the CTLA-4–targeting ICB ipilimumab, with severe irAEs (grade 3 or 4) affecting 24% of these patients (*6*). The irAE rate for anti–PD-(L)1 ICB is 66% overall, with 14% of patients experiencing severe irAEs (*7*). Depending on severity, management of irAEs includes treating symptoms, delaying or stopping ICB treatment, or, in severe cases, administering systemic

[1]Institute of Immunobiology, Kantonsspital St. Gallen, St. Gallen, Switzerland. [2]Sackler Faculty of Medicine, Tel Aviv University, Tel Aviv, Israel. [3]Tel Aviv Sourasky Medical Center, Tel Aviv, Israel. [4]Department of Dermatology, University Hospital Tübingen, University of Tübingen, Tübingen, Germany. [5]Department of Dermatology, Kantonsspital St. Gallen, St. Gallen, Switzerland. [6]Department of Medical Genetics, Life Sciences Institute, University of British Columbia, Vancouver, British Columbia, Canada. [7]Department of Dermatology, University Hospital Zurich, University of Zurich, Zurich, Switzerland. [8]Clinical Collaboration Unit Translational Immunology, German Cancer Consortium (DKTK), Department of Internal Medicine, University Hospital Tübingen, Tübingen, Germany. [9]Interfaculty Institute for Cell Biology, Department of Immunology, University of Tübingen, Tübingen, Germany. [10]Cluster of Excellence iFIT (EXC2180) "Image-Guided and Functionally Instructed Tumor Therapies", University of Tübingen, Tübingen, Germany. [11]German Cancer Consortium (DKTK) and German Cancer Research Center (DKFZ), Partner Site Tübingen, Tübingen, Germany. [12]Department of Oncology and Hematology, Kantonsspital St. Gallen, St. Gallen, Switzerland. [13]Institute of Pathology, University Hospital Bonn (UKB), University of Bonn, Bonn, Germany. [14]Department of Urology, University Hospital Bonn (UKB), University of Bonn, Bonn, Germany. [15]Institute of Experimental Oncology, University Hospital Bonn (UKB), University of Bonn, Bonn, Germany. [16]Institute of Pathology, Kantonsspital St. Gallen, St. Gallen, Switzerland. [17]Department of Oncology, University of Bern, Bern, Switzerland. [18]Division of Oncology, University Hospital Basel, University of Basel, Basel, Switzerland. [19]Department of Cell and Chemical Biology, Oncode Institute, Leiden University Medical Center, Netherlands. [20]Dr. Margarete Fischer-Bosch Institute of Clinical Pharmacology and Robert Bosch Center for Tumor Diseases (RBCT), Stuttgart, Germany.
*Corresponding author. Email: lukas.flatz@med.uni-tuebingen.de
†These authors contributed equally to this work.
‡Deceased.

immunosuppressants (*8*). The occurrence of irAEs can therefore prevent the effective use of ICB, but the real conundrum is that their presence is also associated with enhanced tumor regression and improved survival (*9*). Thus, there is a delicate balance between clinical benefit and autoimmune toxicity. Understanding the mechanisms of both the therapeutic effect of ICB and of the irAEs related to their use may assist in finding the optimal therapeutic window.

Some ICB-induced irAEs occur more often in patients with particular cancer types; for example, vitiligo is much more frequent in patients with melanoma than in other cancers and is associated with improved survival (*10*). This autoimmune skin depigmentation is thought to be caused by T cells that target both melanocytes and melanoma cells expressing the tissue antigens melanocyte lineage-specific antigen (GP100), melanoma antigen recognized by T cell 1 (MART-1), and tyrosinase (*11*). Similarly, pneumonitis—an inflammation of the walls of the alveoli—has a significantly higher incidence in ICB-treated patients with non–small cell lung cancer (NSCLC) compared with, for example, those with melanoma (*12*). At present, there is a lack of validated approaches with which to identify putative antigens shared by tumor and normal tissues that could underlie both irAEs and ICB's antitumor effects. Should such antigens be identified and validated, these findings could then be used to inform mechanistic studies of the distinct or common mechanisms related to antitumor responses and irAE development.

Here, we presented and validated DITAS (discovery of tumor-associated self-antigens), a method enabling the identification of shared tumor and normal tissue antigens that are implicated in ICB responses and irAEs in patients with cancer. We demonstrated the utility of this approach by identifying tumor self-antigens and revealing T cell reactivity against these antigens. Broader application of DITAS may help to further improve ICB therapy by enhancing T cell responses against antigens causing strong antitumor responses and only mild and tolerable toxicity.

RESULTS

DITAS: An approach to identify tumor-associated antigens based on tissue similarities

DITAS combined computational analyses on the basis of transcriptional similarity between lung tumor and healthy lung to identify candidate tumor antigens, with functional T cell assays and single-cell RNA sequencing (RNA-seq) for validation of the antigens. To develop DITAS, we recruited a prospective cohort consisting of 100 patients with stage IV NSCLC and 43 patients with stage IV melanoma treated with ICB. Across the whole cohort, 70.2% of patients received anti–PD-1, 13.2% received anti–PD-L1, 0.7% received anti–CTLA-4, 9.7% received a combination therapy of anti–PD-1 and anti-CTLA-4, and 6.2% received anti–PD-1 in combination with chemotherapy (table S1). A total of 72 patients (50.3%) developed an irAE. The most common irAEs included pruritus (30.8%), skin rash (21.7%), colitis (12.6%), and arthritis (10.5%) (Fig. 1A). In line with previous findings (*9*), patients in the cohort experiencing an irAE had significantly better overall survival (OS) {hazard ratio (HR) = 0.36 [95% confidence interval (CI), 0.25 to 0.54]; log-rank $P < 0.0001$} and progression-free survival (PFS) [HR = 0.38 (95% CI, 0.26 to 0.56); log-rank $P < 0.0001$] compared with patients not developing irAEs (fig. S1).

We found that vitiligo and pneumonitis occurred with markedly different frequencies between patients with melanoma and NSCLC in our cohort. Cases of pneumonitis occurred almost exclusively in patients with NSCLC (12 cases in 100 patients versus 1 case in the 43 patients with melanoma), whereas vitiligo occurred only in patients with melanoma (9 of 43 cases). None of the other irAEs in our cohort showed a marked difference in incidence between the two cancer types (table S2). To validate these findings in data from a larger group of patients, we evaluated whether this difference in specific irAE frequency was also evident in postmarketing safety surveillance reports of ICB-treated cases submitted to the Food and Drug Administration Adverse Event Reporting System (FAERS). This pharmacovigilance database collects spontaneous reports of adverse events (AEs) from which a reporting odds ratio (ROR) (*13*), an indirect surrogate measure of risk of developing an irAE, can be calculated. The higher the ROR, the stronger the association between a drug and an AE. The odds of reporting vitiligo were 15-fold higher in melanoma (ROR, 160.5; 95% CI, 111.1 to 231.9) compared with NSCLC (ROR, 10.6; 95% CI, 4.96 to 22.7), whereas the odds of reporting pneumonitis were threefold higher in NSCLC cases (ROR, 9.44; 95% CI, 8.78 to 10.1) than in melanoma cases (ROR, 3.03; 95% CI, 2.67 to 3.44). This therefore confirmed that the likelihood of vitiligo or pneumonitis was different between the two cancer types, consistent with our patient cohort (Fig. 1B).

We hypothesized that the cancer type–specific development of these ICB-induced autoimmune toxicities might be related to antigenic similarities between the tumor cells and the organ of toxicity. To explore this possibility, we first examined the transcriptional profiles of 400 melanoma samples and 1000 NSCLC samples using the Cancer Genome Atlas (TCGA) (*14*). Then, after selecting genes expressed specifically either in healthy lung tissue or in normal melanocytes according to the existing literature (*15*), we calculated the level of tissue similarity between tumor and nontumor samples on the basis of mRNA expression (see the "DITAS RNA-seq–based bioinformatics analysis" section). As expected, melanoma cells transcriptionally resembled melanocytes (Fig. 1C), whereas NSCLC cells expressed similar genes as lung tissue, although a difference was seen between the adenocarcinoma (AC) and squamous cell carcinoma (SCC) subtypes (Fig. 1D). On the other hand, melanomas did not express lung-specific genes, whereas NSCLCs did not express melanocyte-specific genes (fig. S2). By selecting the 10 melanocyte-specific genes most highly expressed in melanoma, we identified those encoding virtually all known melanocyte differentiation antigens (MDAs), including GP100 (*PMEL*), MART-1 (*MLANA*), tyrosinase (*TYR*), tyrosinase-related protein 1 TRP1 (*TYRP1*), tyrosinase-related protein 2 TRP2 (*DCT*) (*16*), and the more recently described melanoma antigen membrane-associated transporter protein (MATP) (*SLC45A2*) (table S3) (*17*). These antigens are associated with antitumor T cell responses in melanoma and the autoimmune skin toxicity vitiligo (*10*, *11*). We therefore surmised that the same approach could be used to identify candidate NSCLC antigens that might be responsible for lung irAEs and antitumor responses during ICB treatment. Accordingly, we selected the 10 lung-specific genes that were most highly expressed in NSCLC for further study, encoding napsin A (*NAPSA*), uteroglobin (*SCGB1A1*), secretoglobin 3A2 (*SCGB3A2*), surfactant-associated protein 2 (*SFTA2*), surfactant protein A1 (*SFTPA1*), surfactant protein A2 (*SFTPA2*), surfactant protein B (*SFTPB*), surfactant protein C (*SFTPC*), surfactant protein D (*SFTPD*), and sodium-

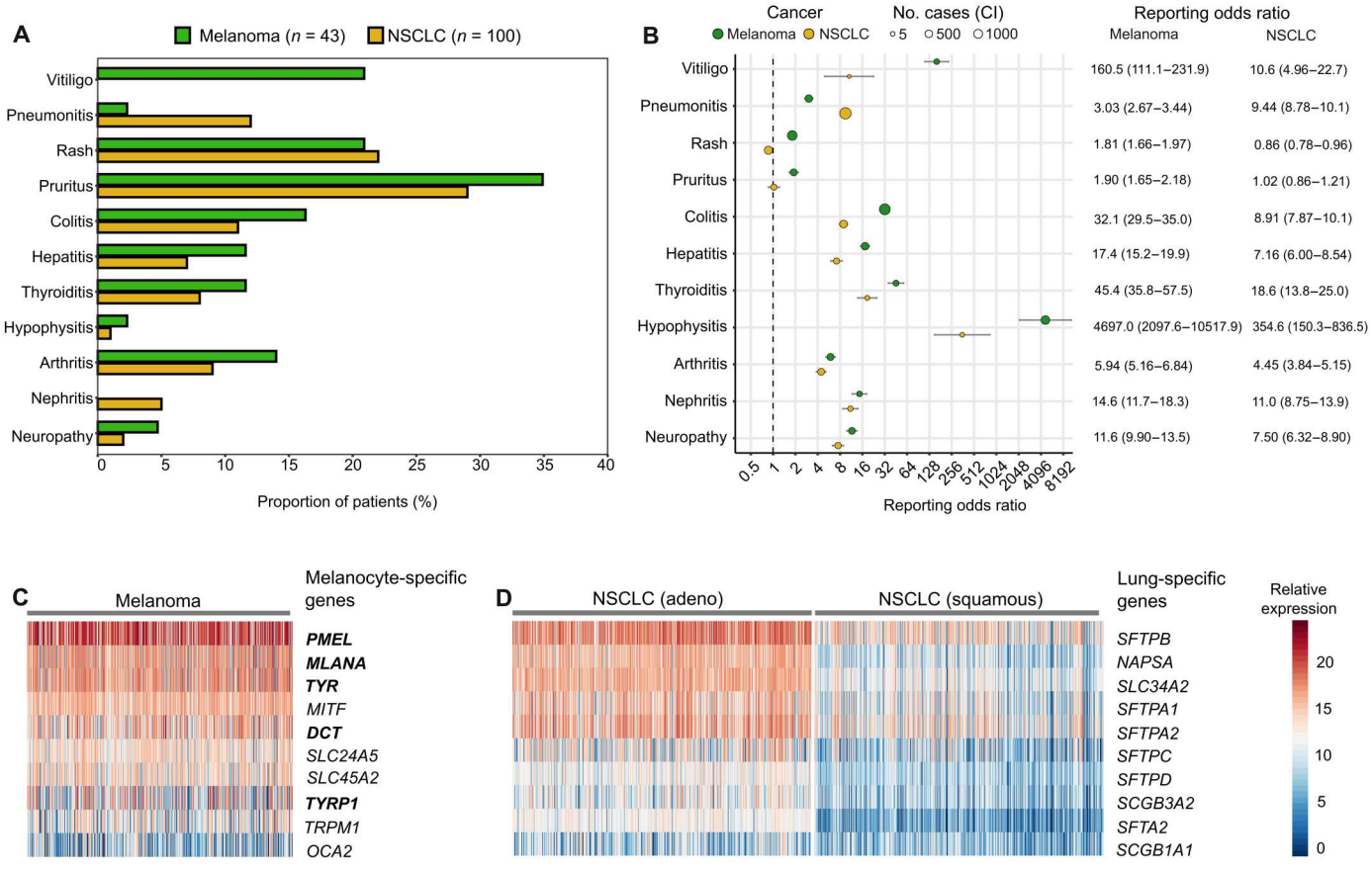

Fig. 1. Frequency of irAEs and relative expression level of tissue-specific genes in melanoma and NSCLC. (**A**) Overview of the irAEs affecting patients with melanoma ($n = 43$) or NSCLC ($n = 100$) in the patient cohort. (**B**) Rates of irAEs in ICB-treated patients ($n = 623'982$) with melanoma or NSCLC according to the FAERS database. The ROR was calculated for ICB-treated cases available in FAERS between July 2014 and January 2020. Circle color indicates cancer type (melanoma or NSCLC), and circle size represents the absolute number of irAE cases. The higher the ROR is, the stronger the association between a drug and AE. (**C** and **D**) RNA-seq analysis of 400 melanoma and 1000 NSCLC samples from TCGA, showing relative expression levels of melanocyte-specific (C) and lung-specific (D) genes. The 10 melanocyte-specific genes mostly highly expressed in melanoma (C) and the 10 lung-specific genes mostly highly expressed in NSCLC (D) are shown. In (C), the genes coding for known MDAs are highlighted in bold.

dependent phosphate transport protein 2B (*SLC34A2*) (table S4). DITAS therefore allowed us to predict promising candidate tumor antigens to be used for subsequent validation experiments.

Validation of napsin A as a lung tumor self-antigen

We next asked whether the predicted proteins encoded by the 10 lung-specific genes identified (Fig. 1 and table S4) were acting as antigens and stimulating T cell responses in patients with NSCLC from our cohort. We first verified that MART-1– and GP100-specific $CD8^+$ T cell responses were significantly greater in patients with melanoma ($n = 33$) compared with those with NSCLC ($n = 18$), using ex vivo peripheral blood mononuclear cell (PBMC) restimulation assays (fig. S3). We also verified that incubation with irrelevant peptide pools did not activate $CD8^+$ T cells (fig. S4). This confirmed that our approach could detect responses to tissue-specific antigens. We then synthesized overlapping 15-nucleotide oligomer peptide pools spanning the entire protein of each of the 10 candidate NSCLC antigens identified in Fig. 1D and used them to perform T cell restimulation assays with PBMCs from patients with NSCLC ($n = 33$). We observed $CD4^+$ (figs. S5, B and C, and S6) and/or $CD8^+$ (Fig. 2A and figs. S5A and S6) T cell responses against all predicted candidate antigens within our NSCLC cohort, suggesting that some of these antigens are immunogenic self-antigens in NSCLC but that recognition of specific antigens varies markedly between patients. In contrast, PBMCs from patients with melanoma ($n = 11$) revealed very few $CD8^+$ T cells responding to the above NSCLC antigens (fig. S7, A and B). However, patients with melanoma showed $CD4^+$ T cell responses toward some candidate antigens (fig. S7, C and D).

In patients with NSCLC, the candidate antigen napsin A—an aspartic proteinase normally expressed in type II pneumocytes of the lung parenchyma (*18*)—was most commonly recognized, showing $CD8^+$ T cell responses in 39% of patients with NSCLC. PBMCs of these patients restimulated with napsin A peptides exhibited frequencies of $CD8^+$ interferon-γ–positive (IFN-γ^+) T cells ranging from 0.2 to 15%, with an average of 0.9% (Fig. 2, B and C). This was not the case in patients with melanoma (Fig. 2C). All patients harboring $CD8^+$ T cell responses toward napsin A expressed human leukocyte antigen (HLA)–A 02:01:01 (table S5). We next confirmed the expression of napsin A in patient lung tumors by performing

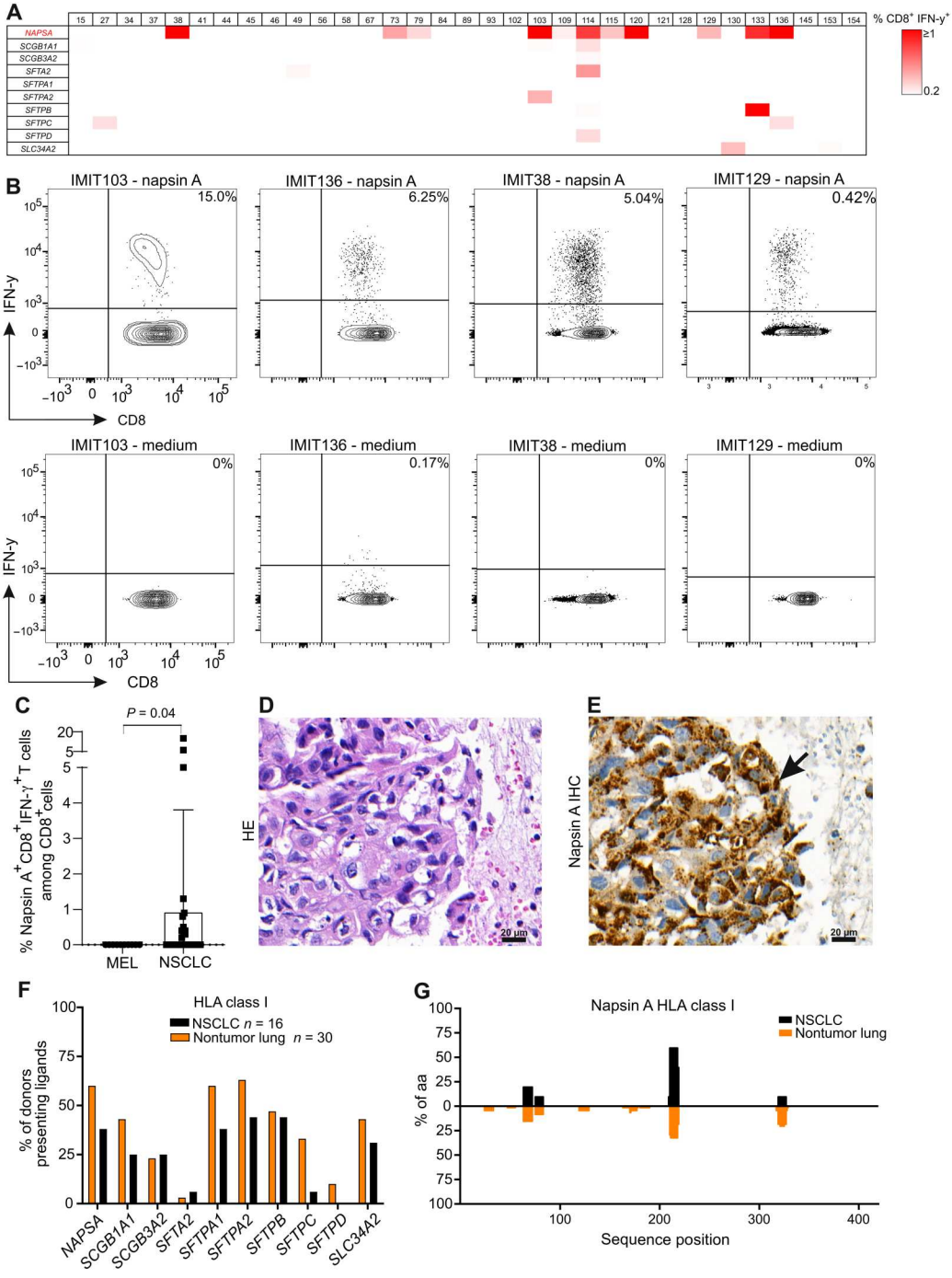

Fig. 2. Peptides from predicted antigens are recognized by CD8⁺ T cells from patients with NSCLC and are naturally presented in the HLA class I immunopeptidome of human lung and NSCLC tissue. (**A**) PBMCs from patients with NSCLC ($n = 33$) undergoing ICB therapy were stimulated individually with peptide pools from the 10 predicted antigens. T cell activation was measured as IFN-γ production by CD8⁺ T cells in the cultures. Each column represents a single patient. The background frequency of CD8⁺ IFN-γ⁺ cells in medium-only negative control cultures was subtracted for all stimulations. (**B**) Representative flow cytometry plots of PMBCs from patients in A stimulated with napsin A peptide pool. Cells were gated on live CD3⁺ CD8⁺ IFN-γ⁺. IMIT numbers refer to patient IDs. (**C**) Frequency of CD8⁺ IFN-γ⁺ cells among total CD8⁺ cells in napsin A–stimulated PBMC cultures from patients with NSCLC ($n = 33$) or melanoma ($n = 10$) (Mann-Whitney test). The background frequency of CD8⁺ IFN-γ⁺ cells in medium-only negative control cultures has been subtracted for all stimulations. (**D**) Hematoxylin and eosin (HE) stain of a NSCLC lymph node metastasis (patient IMIT45), 400×. (**E**) IHC detection of napsin A (strong positive indicated by the arrow) of the lymph node metastasis in (D) (patient IMIT45), 400×. (**F**) Percent of donors presenting HLA class I ligands derived from predicted NSCLC antigens in nontumor lung tissue (orange bars, $n = 30$) and NSCLC tissue (black bars, $n = 16$). (**G**) HLA class I ligand distribution analysis of napsin A protein. Identified peptides were mapped to their amino acid (aa) positions within the source protein. Representation frequencies of amino acid counts within nontumor lung tissues (orange bars) and NSCLC tissues (black bars) for the respective amino acid position (*x* axis) are indicated on the *y* axis. IHC, immunohistochemical.

immunohistochemistry, which showed that napsin A was expressed at the protein level in both NSCLC primary tumors and metastases (Fig. 2, D and E, and fig. S8). We also determined whether patients with NSCLC had antibody responses to napsin A by using their sera to carry out napsin A enzyme-linked immunosorbent assays (ELISAs). This showed that several patients harbored napsin A–specific immunoglobulin G (IgG) antibodies, although there was no correlation between the presence of antibodies and the presence of T cell responses to napsin A in individual patients (fig. S9).

Having detected $CD8^+$ T cell responses to our predicted NSCLC antigens, especially napsin A, we next asked which T cell epitopes within these antigens were being presented by patients' cells in vivo. To achieve this, we eluted the HLA-bound peptides from 30 snap-frozen samples of nontumor lung tissue and 16 snap-frozen samples from NSCLCs and identified them by mass spectrometry. These data represent the tumor immunopeptidome and revealed that naturally presented HLA class I ligands derived from all 10 of our predicted antigens were present in nonmalignant lung tissue and from 9 of 10 of the predicted antigens on lung tumor cells (Fig. 2F and table S6). Most of the HLA class I ligands derived from the predicted antigens, especially from napsin A, were identical between nontumor lung tissue and NSCLC, showing that they are true self-epitopes (Fig. 2G and fig. S10). Together, these data showed that DITAS identified candidate tumor antigens that elicited $CD8^+$ T cell activation and were naturally presented on lung tumor cells.

Functional relevance of napsin A–specific T cells

We next aimed to assess the potential of the DITAS approach to identify common tumor/tissue antigens that exhibit key features of functional relevance to antitumor immunity and/or irAEs. Relevant antigens should be able to stimulate the activation and proliferation of $CD8^+$ T cells in patients responding to therapy, trigger cytotoxic activity toward tumor cells presenting that antigen, and be recognized by T cells from within the tumor. Moreover, T cells specific for tumor antigens should have a proinflammatory and cytotoxic gene signature. Because napsin A was the most commonly recognized antigen and also elicited the highest $CD8^+$ T cell restimulation responses ex vivo, we focused on this protein for subsequent experiments.

First, we assessed whether differences in the frequency of napsin A–specific T cells were present between patients with NSCLC responding to therapy compared with those not responding well. When we measured the frequency of napsin A–specific $CD8^+$ T cells in blood from ICB-treated patients after stimulation with a napsin A peptide pool, we found that responders to ICB harbored significantly higher frequencies compared with nonresponders (Fig. 3A). Our data also suggested an association between the presence of an ex vivo $CD8^+$ IFN-γ^+ response upon napsin A stimulation and prolonged OS (fig. S11A) and PFS (fig. S11B) of patients with NSCLC, although these data were not significant. We did not detect any association between the presence of napsin A–specific IgG antibodies and survival in patients with NSCLC (fig. S12).

To complement the naturally presented peptides identified above for use in our assays, we also predicted napsin A nonamer and decamer peptides for HLA-A 02:01 [one of the most frequent HLA class I allotypes in humans (*19*) and the one expressed by all patients harboring anti–napsin A $CD8^+$ T cell responses (table S5)]. We then carried out T cell stimulation assays with peptides representing the predicted epitopes and with napsin A peptides from the immunopeptidomic dataset of NSCLC and nontumor lung tissue (fig. S13 and table S7). We identified several napsin A $CD8^+$ T cell epitopes capable of activating cells from ICB-treated patients with NSCLC, two of which are also naturally HLA-presented on lung tissue (Fig. 3B).

Having shown that napsin A–derived peptides could activate T cells from patients with NSCLC, we next wondered whether napsin A could also elicit $CD8^+$ T cell proliferation and antitumor T cell responses ex vivo. We found that PBMC cultures incubated with napsin A contained significantly higher frequencies of proliferating $CD8^+$ T cells than did medium-only control cultures (Fig. 3C) and that these $CD8^+$ T cells could kill immortalized napsin A–pulsed NSCLC cells of matching HLA I type in coculture (Fig. 3D and fig. S14). For such napsin A–specific $CD8^+$ T cells to either execute irAEs or antitumor responses in patients with NSCLC, they would need to be present within this tissue. We confirmed, using HLA-A 02:01 tetramers loaded with the napsin A epitopes from Fig. 3B, that we could detect napsin A–specific $CD8^+$ T cells in PBMCs and lung tumors of patients (Fig. 3, E and F).

To validate the presence of napsin A–specific T cells in human lung tumors, we verified whether napsin A–specific T cell receptors (TCRs) were present within the tumors and inflammatory lung lesions of patients with NSCLC treated with ICB. First, we incubated PBMCs from four patients with napsin A peptides and sorted $CD8^+$ IFN-γ^+/tumor necrosis factor–positive (TNF^+) T cells from the culture. We then performed TCR sequencing of the DNA from the sorted napsin A–specific T cells and compared them with the TCR sequences of T cells present in formalin-fixed paraffin-embedded (FFPE) samples of NSCLCs and ICB-induced inflammatory lung lesions or within PBMCs. Several of the napsin A–specific T cell clones circulating in the blood were present in the lung tumors and inflammatory lesions of patients, with some sequences being shared among patients (table S8). Furthermore, we found that napsin A–specific TCR sequences were significantly enriched in lung tumors and inflammatory lung lesions compared with the peripheral blood (fig. S15). To verify these findings in a larger patient population, we investigated whether the identified napsin A–specific TCRs were present in a publicly available TCR database containing TCR sequences from NSCLCs and other tumor types as well as from the blood of patients with NSCLC. This confirmed that napsin A–specific TCRs were significantly enriched in NSCLC tumors compared with melanomas (Fig. 4A) and compared with the blood of patients with NSCLC (Fig. 4B).

Next, to validate the functionality and the cytotoxic potential of napsin A–specific T cells, we performed single-cell RNA-seq of activated $CD8^+$ T cells from PBMCs of patients after stimulation with a napsin A peptide pool. We found that napsin A–specific T cells expressed proinflammatory markers, including IFN-γ and TNF, and the cytotoxic markers granzyme B, perforin, and Fas ligand (Fig. 4, C and D, and fig. S16). When comparing the TCR sequences of these proinflammatory and cytotoxic napsin A–specific T cell clonotypes sorted from patient blood with patient-matched lung tumors, we found that several of these clonotypes were shared with the tumor (Fig. 4E), further suggesting a clinical relevance of these T cell clones.

Together, these results indicated that DITAS allowed the identification of a key tumor relevant self-antigen, napsin A. Napsin A was recognized by specific $CD8^+$ T cells with proliferative and cytotoxic potential that were enriched in the lung tumors and

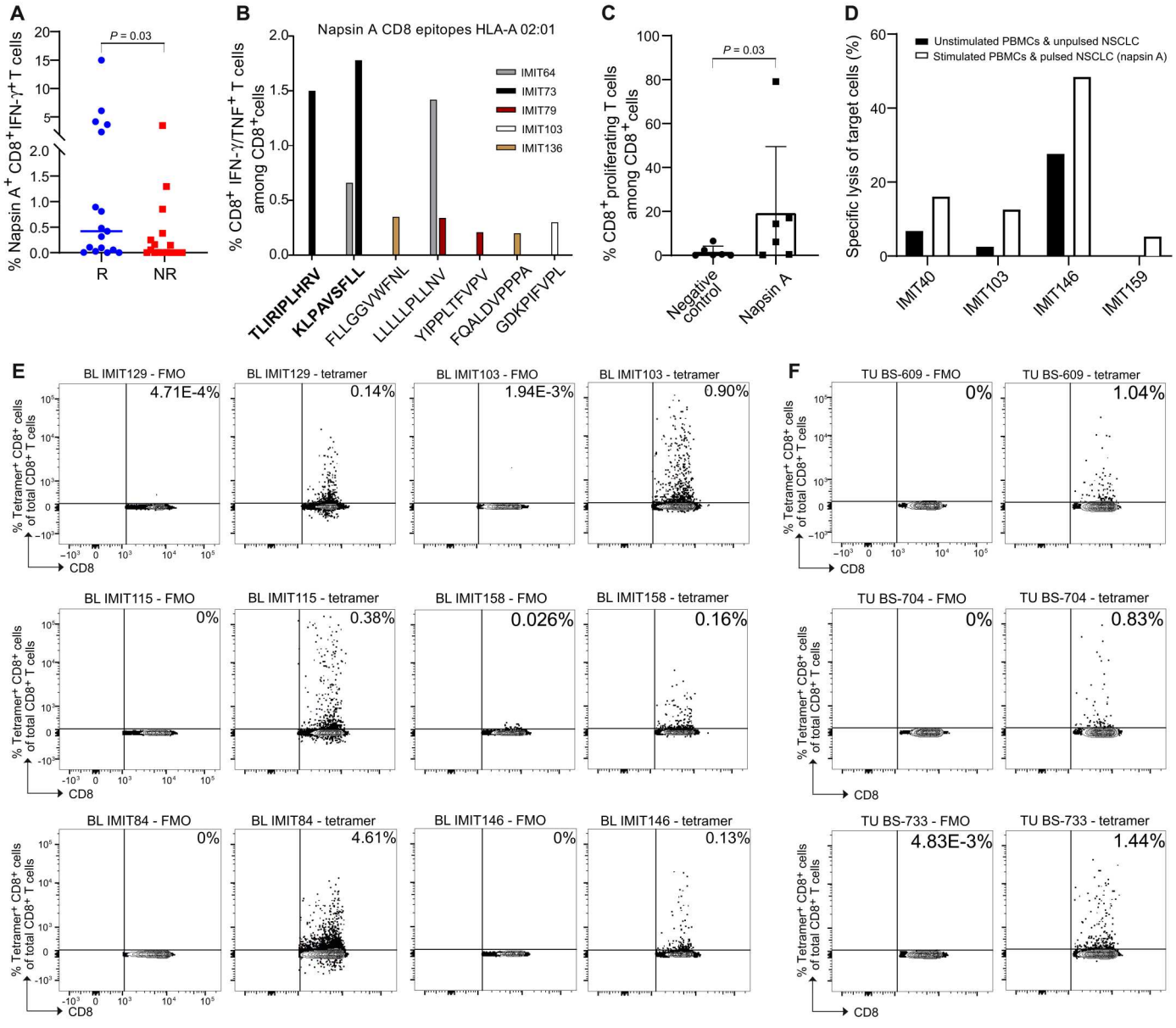

Fig. 3. Napsin A–specific CD8⁺ T cells are found in the blood and tumors of patients with NSCLC with higher frequencies in patients responding to therapy. (**A**) Frequency of napsin A–specific CD8⁺ IFN-γ⁺ T cells in the blood of patients with NSCLC responding to ICB therapy (responder, R) ($n = 17$) versus those not responding to therapy (non-responder, NR) ($n = 17$) (Mann-Whitney test). (**B**) Identification of napsin A CD8⁺ T cell epitopes in HLA-A 02:01 patients with NSCLC treated with ICB therapy after PBMC stimulation with individual epitopes. Epitopes highlighted in bold were also found in the HLA ligandome of NSCLCs. (**C**) PBMC cultures from patients with NSCLC ($n = 6$) undergoing ICB therapy were stimulated with napsin A. The frequency of proliferating CD8⁺ T cells was measured after 7 days (Wilcoxon test). (**D**) PBMC cultures from patients with NSCLC ($n = 4$) were stimulated with napsin A and cocultured overnight with a napsin A–pulsed immortalized NSCLC cell line of matching HLA class I type. The following day, the frequency of NSCLC cell death was analyzed using the Apotracker green/propidium iodide apoptosis detection kit. (**E** and **F**) PBMCs from patients with NSCLC [$n = 6$, (D)] and NSCLC single-cell suspensions [$n = 3$ (E)] were incubated with a pool of seven napsin A tetramers [sequences are shown in (B)]; fluorescence minus one (FMO) stains were used as negative controls. IMIT (IMIT patient cohort) and BS numbers refer to patient IDs.

inflammatory lung lesions of ICB-treated patients with NSCLC. Our experimental pipeline might be applicable to other tumor types to inform what antigens might induce irAEs during ICB (Fig. 5).

DISCUSSION

During autoimmune reactions, healthy tissues are no longer identified by the immune system as "self," leading to a breach of tolerance and subsequent tissue destruction. In the case of ICB-induced irAEs, T cells are thought to be the major mediators of this destruction, because their activity is directly enhanced by ICB treatment (*20*). There are two leading hypotheses that may explain the

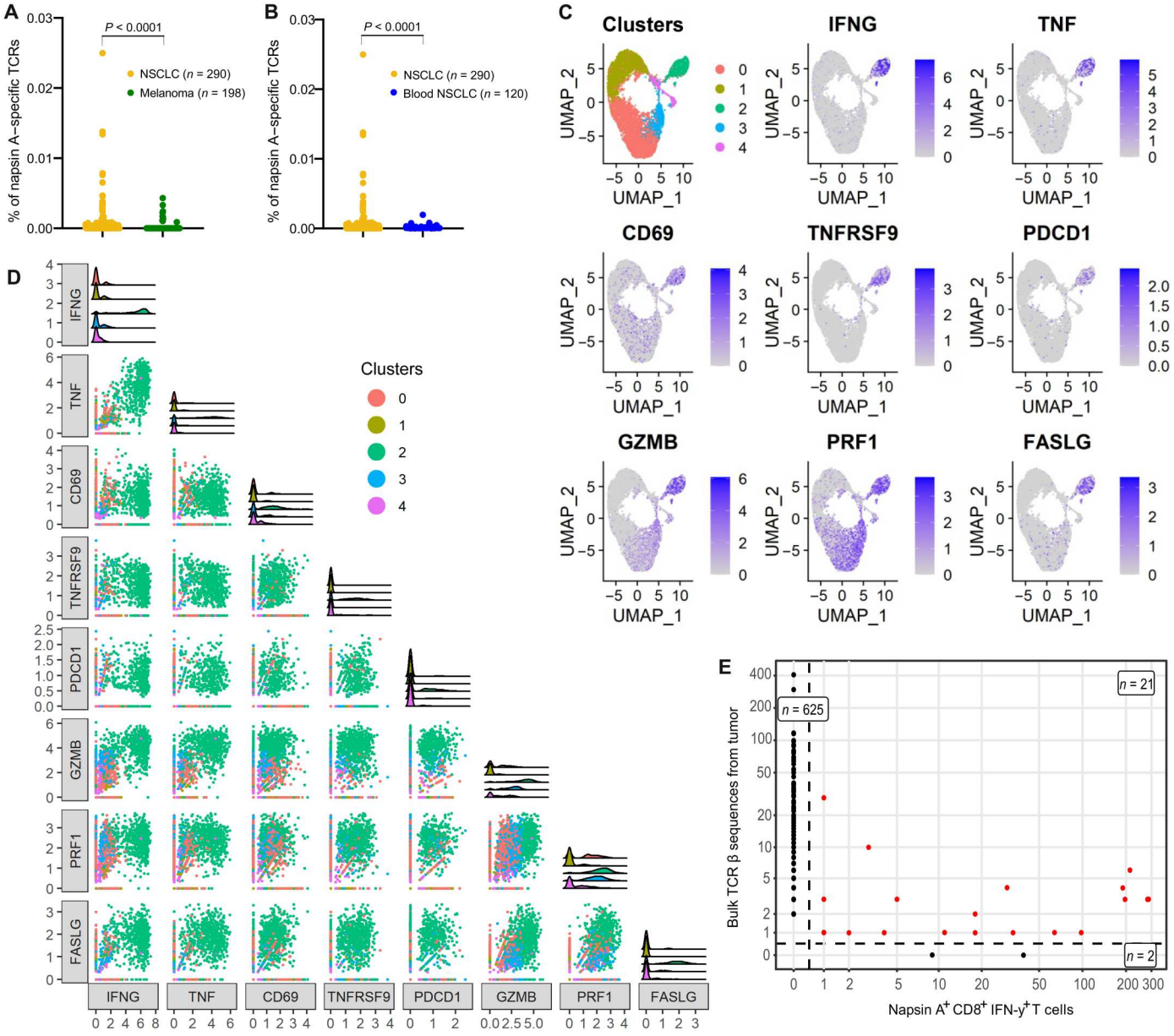

Fig. 4. Napsin A–specific CD8+ T cells are significantly enriched in lung tumors and express cytotoxic markers. (**A** and **B**) Napsin A–specific T cells were sorted from the blood of ICB-treated patients with NSCLC after stimulation with a napsin A peptide pool, and DNA was extracted for TCR sequencing. A publicly available TCR database (see the "Analysis of napsin A–specific TCR expression using a publicly available TCR database" section) was then used to establish the frequency of napsin A–specific TCR sequences in NSCLC tumors (n = 290), melanomas (n = 198), and the blood of patients with NSCLC (n = 120) (Mann-Whitney test). (**C**) UMAP plots showing single-cell transcriptomic profiles of sorted napsin A–specific CD8$^+$ T cells from two patients with NSCLC treated with ICB therapy and the single-cell expression of key marker genes of napsin A–specific cytotoxic T cells. (**D**) Plot matrix of scatter and ridgeline plots showing coexpression of cytokines in napsin A–specific CD8$^+$ T cells. (**E**) TCR β chain sequences of the proinflammatory and cytotoxic single-cell sequencing cluster [napsin A–specific clones, cluster 2 from (C)] were compared with TCR β chain sequences obtained from tumor-infiltrating lymphocytes. Common specificities shared between napsin A–specific clones sorted from blood and clones found in tumors (shown in red) were inferred using GLIPH2 (*47*). UMAP, uniform manifold approximation and projection.

breach in regulation of T cell activity that occurs during ICB treatment: the neoantigen theory and the tissue-associated antigen theory. In support of the former, studies in humans indicate that T cells targeting cancer neoantigens may cross-react with the corresponding wild-type version of the protein (*21*). On the other hand, there is also evidence for the tissue-associated antigen theory: Antigen sharing between tumors and healthy tissue may explain associations between clinical outcome during immunotherapy and the presence of autoimmune toxicity because cytotoxic T cells targeting self-antigens are expressed in both tissues (*22*, *23*). What therefore becomes apparent is that the antigens targeted in ICB-induced irAEs might be important drivers of the antitumor response, and so identifying them could reveal targets expressed by

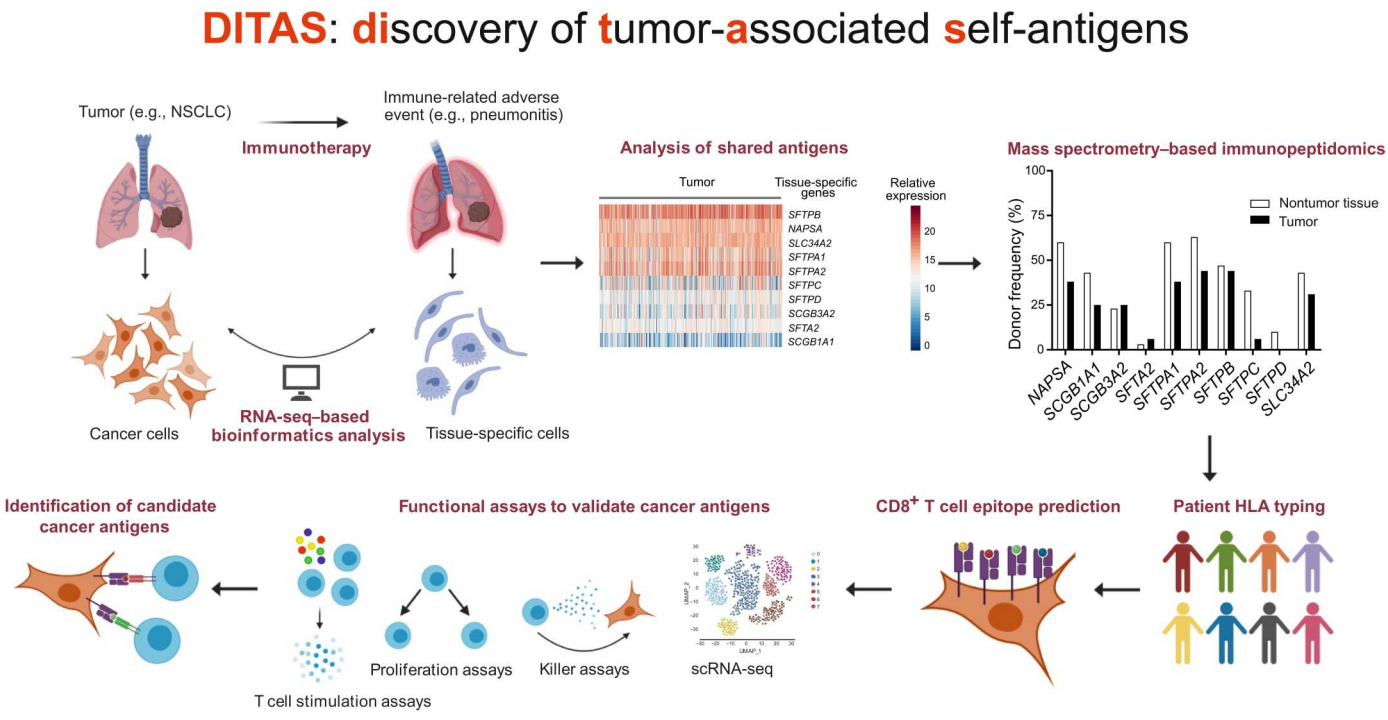

Fig. 5. Pipeline for the identification of candidate tumor–associated antigens. ICB-induced irAEs can be exploited to identify candidate tumor antigens. The first step involves comparing the transcriptional-level tissue similarity between the tumor and the nontumor tissue affected by the toxicity and then selecting the nontumor tissue-specific genes that are most highly expressed in the tumor. Mass spectrometry–based immunopeptidomics can then be used to determine the frequency of naturally presented HLA class I and class II ligands derived from the predicted tumor antigens. $CD8^+$ T cell epitope prediction followed by a variety of functional assays [e.g., T cell stimulation assays, cytotoxicity assays, TCR sequencing, and single-cell RNA-seq (scRNA-seq)] allows for the identification of specific $CD8^+$ T cell epitopes and for further validation of the candidate tumor antigens.

tumors and potentially improve the future design of ICB-based therapies with fewer side effects.

Here, we described a pipeline called DITAS for the identification of antigens with potential relevance for ICB-induced antitumor responses and for ICB-associated irAEs. Comparing antigenic similarities between lung tumors and irAE-affected nontumor lung tissues yielded 10 candidate tumor antigens. We verified these by T cell stimulation assays, proliferation assays, and target cell lysis assays, followed by further characterization using TCR sequencing and single-cell RNA-seq. We showed how DITAS combined a bioinformatics-based approach with functional assays to identify candidate T cell tumor antigens with a strong likelihood of mediating both antitumor responses and irAEs. This pipeline might be applicable to multiple cancer types and anticancer therapies but needs testing in other situations. The validation of this method showed its ability to identify all established MDAs, which have also been found in the immunopeptidome of melanoma and can elicit strong antitumor responses (*24*). Our pipeline then defined 10 candidate NSCLC tumor antigens shared between NSCLC and healthy lung tissue, and our data suggested that napsin A, in particular, is a promising NSCLC antigen. We further characterized multiple HLA ligands derived from these antigens by mass spectrometry–based immunopeptidome analysis of NSCLC and nontumor lung tissue, representing an unbiased approach to determine natural presentation of tumor-associated antigens (*25*).

A pipeline of technologies as presented here is urgently needed: To date, few NSCLC antigens have been identified (*26*). Further studies in larger cohorts and detailed mechanistic investigations will be required to determine whether napsin A and the other antigens identified have widespread clinically relevant antitumor and irAE potential and, if so, how to exploit or control it. Although napsin A has not yet been associated with autoimmunity, it is highly expressed in lung ACs and is now used as a marker to distinguish lung AC from lung SCC. In addition, the absence of napsin A expression in lung ACs is a poor prognostic factor (*18*). Napsin A is therefore likely to drive antitumor responses and lung irAEs in lung AC rather than in lung SCC. Here, we showed that patients with NSCLC responding to ICB had significantly higher frequencies of napsin A–specific $CD8^+$ IFN-γ^+ T cell responses compared with nonresponders. This was further corroborated by the identification of napsin A–specific T cell clones in both lung tumors and inflammatory lung lesions of ICB-treated patients and the fact that napsin A–specific TCRs were enriched in lung tumors compared with other tumors and peripheral blood. The presence of autoimmune T cells specific for napsin A and other self-antigens does not necessarily imply that patients will develop inflammatory lesions such as pneumonitis, but these autoreactive T cells may still show an antitumor effect. A similar phenomenon is observed in melanoma, where many patients harbor MDA-specific T cells in their tumors and blood, whereas few of these patients develop vitiligo (*10*). The presence of autoreactive lymphocytes alone is likely insufficient to cause autoimmune AEs, and several other factors, including a proinflammatory environment and host genetics, are likely to play important roles (*27*). However, the unleashing of these autoreactive

T cells by ICB treatment may allow immune responses against tissues and associated tumors alike. Accordingly, many studies have shown that patients with cancer experiencing autoimmune side effects during ICB therapy have improved survival (*9*). What remains extremely challenging is dissecting survival effects linked to specific types of irAEs because most patients develop several simultaneously rather than just one. This limitation also affected our study because it was not possible to analyze the association of pneumonitis and survival in a suitably large cohort. In addition, despite the promising role of autoreactive T cells and self-antigens in fighting cancer, great caution must be implemented when considering their potential in anticancer therapies because of the associated risk of autoimmune toxicities. Future studies might explore this risk first in animal models, which can be informative about the safety profile and tolerability of cancer therapies exploiting self-antigens.

The definition of tumor T cell targets will help to further improve cancer immunotherapies. The DITAS approach may help identify targetable tumor-specific antigens. The identification of tumor antigens targeted in ICB therapy also helps improve our understanding of the mechanism behind ICB and its irAEs, because there is now very limited knowledge related to the antigen specificity of T cells mediating antitumor responses and irAEs during ICB treatment.

MATERIALS AND METHODS

Study design

The research objectives of this study were (i) to develop an approach to identify tumor self-antigens in ICB-treated patients with NSCLC and (ii) to validate the identified cancer antigens and determine whether they play a role in antitumor responses and lung irAEs. Samples for this study were obtained from a prospective cohort study of patients with stage IV NSCLC starting therapy with ICB (described below). Our approach consisted of two parts: an initial step based on computational transcriptional similarity scores (to identify the candidate antigens) and a second validation step based on functional T cell assays, mass spectrometry–based immunopeptidomics, TCR sequencing, and single-cell RNA-seq. The functional T cell assays consisted of T cell stimulation assays, $CD8^+$ T cell epitope prediction, tetramer in-house generation and staining, proliferation assays, and target cell lysis assays.

Clinical sample collection

A prospective cohort study [immunomonitoring of immunotherapy (IMIT) study] of patients with stage IV NSCLC ($n = 100$) or melanoma ($n = 43$) who received ICB treatment was conducted across four clinical centers in Switzerland (Kantonsspital St. Gallen, Spital Grabs, Spital Wil, and Spital Flawil) from 1 July 2016 to 1 October 2020. The study received ethical approval from the Ethikkommission Ostschweiz. Written informed consent was obtained from all patients. Blood was collected, and PBMCs were isolated for analyses, with patient follow-up after 1 year. Serum was also collected from all patients. From some patients, FFPE tumor tissues from the remaining tumor resections and diagnostic biopsies were used for TCR sequencing analyses.

Immunopeptidome data generated from snap-frozen human lung tumors and human nontumor lung samples (*28*) were provided by the University of Tübingen, Germany.

TCR sequencing data from human ICB-induced inflammatory lung lesions were provided by the University of Basel, Switzerland. All human samples were collected with ethical approval and patient written informed consent in accordance with the Declaration of Helsinki guidelines.

Isolation of PBMCs

Patient blood was collected in EDTA-containing tubes, and PBMCs were isolated following standard Ficoll-Paque density gradient separation. After isolation, PBMCs were cryopreserved at −150°C in RPMI medium containing 10% dimethyl sulfoxide (DMSO).

DITAS RNA-seq–based bioinformatics analysis

To define tissue- or cell-specific genes, we analyzed previously published RNA-seq datasets. Genes expressed at a high level (at least fivefold more mRNA than in other tissues) specifically in human lung were identified using the Human Protein Atlas (*29*). Melanocyte-specific genes were defined using raw data from Reeman *et al.* (*15*), who performed a whole-transcriptome analysis of the main human skin cell types. If a gene had RPKM (Reads Per Kilobase Million) > 100 in melanocytes and significantly higher expression in melanocytes compared with keratinocytes, fibroblasts, or whole skin, then the gene was considered melanocyte-specific. The melanocyte-specific gene *MITF* was added on the basis of the existing literature (*30*). Next, raw data from 443 melanoma samples and 994 NSCLC samples (510 AC type and 484 SCC type) were obtained from TCGA repository (*14*). A transcriptional similarity score between the TCGA samples and lung tissue or melanocytes was calculated via single-sample gene set enrichment analysis in the GSVA R package (*31*), using healthy lung- or melanocyte-specific genes as gene sets.

Pharmacovigilance analysis

Postmarketing AE cases in 623,982 patients with cancer undergoing therapy with ICB or other cancer medications between 1 July 2014 and 31 December 2019 were extracted from the U.S. FAERS. To approximate the risk of patients with melanoma or NSCLC developing the irAE of interest, we estimated the ROR (*13*) by comparing the odds of reporting the selected irAEs rather than other AEs under ICB therapy, with the reporting odds of all other drugs in the database. This method is the standard practice for quantitative analyses of data in FAERS and similar pharmacovigilance databases (*13*).

Preparation of peptide pools

Peptide pools were ordered from GenScript in the form of lyophilized 15 nucleotide oligomers with five–amino acid overlap or as single nonamer and decamer peptides. Peptide purity was >85%. Peptide pools were dissolved in DMSO, diluted in RPMI, aliquoted, and stored at −20°C.

T cell stimulation assays and flow cytometry

Cryopreserved PBMCs were plated at a concentration of 1×10^6 cells per well in low-adherence 24-well plates (Sarstedt, reference no. 83.3922.500) and maintained at 37°C. Cells were resuspended in 2 ml of RPMI per well containing 8% human serum (Biowest, ref. S4190-100), 1% penicillin-streptomycin, 1% L-glutamine, 1% nonessential amino acids, 1% sodium pyruvate, kanamycin (0.1 mg/ml), and 0.1% 2-β-mercaptoethanol. The following day, peptide pools or single peptides were added at a final concentration of 2

μg/ml per peptide. After 48 hours, 1 ml of medium was replaced with fresh RPMI (as above) containing interleukin-2 (IL-2; final concentration of IL-2 was 150 U/ml). Cells were kept in culture for 10 days, and 1 ml of medium was replaced with fresh IL-2–containing medium every second day. On day 10, cells were collected from the plates, washed, and transferred to 96-well plates, where they were restimulated with peptide(s) for 6 hours in the absence of IL-2 at a concentration of 2 μg/ml per peptide. Brefeldin A was added at the same time at a final concentration of 10 μg/ml. After 6 hours, cells were washed, stained for viability, and incubated with fluorescently labeled antibodies recognizing CD3–allophycocyanin (APC)–Cy7 (BioLegend, catalog no. 317342), CD4–phycoerythrin (PE)–Cy7 (BioLegend, catalog no. 317414), CD8-PerCP (BioLegend, catalog 344708), and CD45RA-BV711 (BioLegend, catalog no. 304138) in fluorescence-activated cell sorting (FACS) buffer. Cells were then fixed and permeabilized using BD Cytofix/Cytoperm and incubated with fluorescently labeled antibodies recognizing IFN-γ–PE (Invitrogen, catalog no. MHCIFG04) and TNF-APC (BioLegend, catalog no. 502912) in Perm buffer. Samples were acquired using the BD LSRFortessa flow cytometer, and data were analyzed using the FlowJo software. IFN-γ and TNF production were analyzed to identify antigen-specific T cells. For some patients, $CD8^+$ IFN-γ^+ T cells were sorted using the BD FACSMelody, and DNA was extracted and used for TCR sequencing (see below).

HLA immunoaffinity purification

HLA class I and II molecules were isolated from snap-frozen tissue by a standard immunoaffinity chromatography (*32*) using the monoclonal antibodies W6/32, Tü39, and L243.

Mass spectrometric data acquisition

HLA ligand extracts were analyzed as described previously (*28*, *33*). Peptides were separated by nanoflow high-performance liquid chromatography. Eluting peptides were analyzed on an on-line coupled Orbitrap Fusion Lumos and/or an LTQ Orbitrap XL mass spectrometer (both Thermo Fisher Scientific, San Jose, CA).

Mass spectrometric data processing

Data processing was performed as described previously (*32*) using the Proteome Discoverer software (v1.4, Thermo Fisher Scientific, San Jose, CA) to integrate the search results of the SEQUEST HT search engine (University of Washington) (*34*) with the human proteome (Swiss-Prot database). The false discovery rate estimated by the Percolator algorithm 2.04 (*35*) was limited to 5% for HLA class I and 1% for HLA class II. HLA class I annotation was performed using SYFPEITHI 1.0 (*36*) and NetMHCpan 4.0 (*37*).

Haplotype sequencing

High-resolution (4×) HLA haplotyping was performed using next-generation sequencing (HistoGenetics, New York, USA) of cryopreserved PBMCs. With this technology, complete HLA class I (A, B, and C) genes were sequenced, resulting in six-digit allele-level HLA types.

CD8 epitope prediction

CD8 T cell epitopes for napsin A were predicted for HLA-A 02:01. MHC class I binding prediction was performed with IEDB (Immune Epitope Database Analysis Resource) on the basis of MHC class I binding affinity. Nonamers and decamers with the highest immunogenicity scores were selected for peptide synthesis (percentile rank < 1.5%, median inhibitory concentration < 160 nm). The peptides were synthesized by GenScript and had >85% purity. Lyophilized peptides were dissolved in DMSO, diluted in RPMI, aliquoted, and stored at −20°C.

Labeling of T cells with napsin a tetramers

Napsin A tetramers for HLA-A 02:01 were produced in-house using temperature exchange as previously described (*38*, *39*) and the epitope sequences identified in Fig. 3B (TLIRIPLHRV, KLPAVSFLL, FLLGGVWFNL, LLLLLPLLNV, YIPPLTFVPV, FQALDVPPPA, and GDKPIFVPL). PBMCs and tumor single-cell suspensions were thawed the day before the experiment and kept at 37°C overnight. The following day, they were stained to assess viability and then incubated with PE-labeled napsin A tetramers (1:40) for 10 min at 37°C in FACS buffer. Cells were then washed and incubated with fluorescently labeled antibodies recognizing CD3-APC-Cy7 (BioLegend, catalog no. 317342) and CD8-PerCP (BioLegend, catalog no. 344708) in FACS buffer. Samples were acquired using the BD LSRFortessa flow cytometer, and data were analyzed using the FlowJo software.

Napsin A ELISA

Recombinant napsin A was produced in-house using human embryonic kidney 293 cells and affinity-purified. For coating of the ELISA plate wells, napsin A (0.5 μg/ml) in 50 μl of carbonate buffer (pH 9.5) was used per well and incubated at 4°C overnight. On the following day, the plates were washed, blocked using 200 μl of ELISA diluent (5× ELISA/ELISPOT diluent; Thermo Fisher Scientific), and incubated at room temperature overnight. Patient serum was diluted 1:100 in ELISA diluent, then 50 μl of the diluted serum was transferred to the ELISA plate and incubated for 2 hours at room temperature. Next, 50 μl of 1:1000 goat antihuman IgG horseradish peroxidase (Jackson ImmunoResearch, catalog no. 109-035-003) was added and incubated for 1 hour at room temperature. After washing with phosphate-buffered saline (PBS), we added 100 μl of trimethylboron ELISA substrate (catalog no. 3652-F10; Mabtech AB, Stockholm, Sweden), and the plates were incubated in the dark at room temperature. The reaction was stopped with 20 μl of 2.5 N sulfuric acid solution. The light absorption at 450 nm was measured in a Sunrise absorbance microplate reader (Tecan, Männedorf, Switzerland).

Histological evaluation of napsin A expression in lung tumors

Tumor tissue availability at the Kantonsspital St. Gallen was evaluated for all patients included in this study. For 18 patients, there were FFPE blocks available with sufficient material of good quality to detect napsin A. From one patient, healthy lung tissue could also be obtained, which was used as a positive control. Sections were incubated with napsin A antibody (Leica Biosystems, Wetzlar, Germany) at a concentration of 1:400 on a Leica BOND III platform according to the previously established protocols used in routine diagnostics. The labeling pattern was evaluated by a certified pathologist and categorized into "negative," "weak," or "strong." The histological slides were scanned on a Pannoramic 250 Flash III scanner (3DHISTECH, Budapest, Hungary).

Target cell lysis assay

PBMCs were counted and plated at a concentration of 1×10^6 cells per well in low-adherence 24-well plates in 2 ml of RPMI containing 8% human serum, 1% penicillin-streptomycin, 1% L-glutamine, 1% nonessential amino acids, 1% sodium pyruvate, kanamycin (0.1 mg/ml), and 0.1% 2-β-mercaptoethanol. After overnight incubation at 37°C, peptide pools or single peptides were added to wells at a final concentration of 2 μg/ml per peptide. After 48 hours, 1 ml of medium was replaced with fresh RPMI (as above) containing IL-2 (final concentration of IL-2 was 150 U/ml). Cells were kept in culture for 10 days, and 1 ml of medium was replaced with fresh IL-2 containing medium every second day. On day 10, cells were collected, washed, and transferred to 96-well plates before restimulation with peptide(s) for 6 hours in the absence of IL-2 at a final concentration of 2 μg/ml per peptide. Simultaneously, target cells (NSCLC cell line HCC2935, HLA-A 02:01) were stained with an APC-labeled cell dye (eBioscience catalog no. 65-0840), and half of the target cells were then also pulsed with the same peptide(s) for 2 hours at a final concentration of 2 μg/ml per peptide. Incubation with 100 μM doxorubicin was used as a positive control. PBMCs and target cells were then cocultured overnight in round-bottom 96-well plates in RPMI at an effector-to-target ratio of 10:1 or 30:1. The following day, an apoptosis assay was carried out using an Apotracker green/PI kit to determine target cell death. Data were acquired using an BD LSRFortessa flow cytometer and analyzed using the FlowJo software.

Proliferation assay

Cryopreserved PBMCs were stained with carboxyfluorescein diacetate succinimidyl ester in PBS for 20 min at 37°C and then stimulated with peptide pools or single peptides at a final concentration of 2 μg/ml per peptide. Cells were then cultured for 10 days, with the addition of IL-2 (100 U/ml) every other day. After 10 days, cells were incubated with fluorescently labeled antibodies against CD3-APC (BioLegend, catalog no. 300312), CD4-PE-Cy7 (BioLegend, catalog no. 317414), CD8-PerCp (BioLegend, catalog no. 344708), and CD45RA-BV711 (BioLegend, catalog no. 304138) in FACS buffer. Data were acquired using a BD LSRFortessa flow cytometer and analyzed using the FlowJo software.

TCR β sequencing

DNA was extracted from ICB-treated NSCLC samples and inflammatory lung lesions (FFPE samples) and from sorted PBMCs (see the "T cell stimulation assays and flow cytometry" section). The DNA was used to carry out TCR β sequencing (ImmunoSEQ "Survey" resolution, Adaptive Biotechnologies). Clonotypes represent unique genomic nucleotide sequences resulting from V, D, and J gene rearrangement. The data were analyzed using the Adaptive Biotechnologies Analyzer platform.

Analysis of napsin A–specific TCR expression using a publicly available TCR database

Public projects for which TCR sequences of tumor and blood samples of patients with NSCLC (*40*, *41*) and melanoma (*42*, *43*) were made available online were chosen using the TCR database TCRdb (http://bioinfo.life.hust.edu.cn/TCRdb/#/). The TCR sequences generated during these projects were reposited on the ImmunoSeq Analyzer platform, which was used to conduct the search for specific clonotypes. By using the CMV search tool, we identified clones with matching sequences in each sample and retrieved their total productive frequency, which was then compared between the different compartments and tumor types.

Processing of samples for single-cell RNA-seq

Human PBMCs were stimulated with napsin A peptides and cultured for 10 days. Sorted live $CD3^+CD8^+CD137^+$ human T cells (CD3-FITC, BioLegend, catalog no. 317306; CD8-PerCP, BioLegend, catalog no. 344708; CD137-APC, BioLegend, catalog no. 309810) were run using the 10x Chromium (10x Genomics) system, and cDNA libraries were generated according to the manufacturer's recommendations (Chromium NextGEM Single Cell 5′ Reagent Kits v2) and sequenced via Illumina NovaSeq 6000 at the Functional Genomic Center Zurich.

For the TCR repertoire, cDNA libraries generated from Chromium NextGEM single-cell 5′ reagent kits were further processed with the Chromium single-cell human TCR amplification kit to enrich the TCR region. TCR libraries were sequenced with Illumina NextSeq 500 at the Functional Genomic Center Zurich. Sequenced files were preprocessed using CellRanger.

Single-cell gene expression analysis

Single-cell gene expression analysis was performed using Seurat V. 4.0.4 (*44*). Low-quality cells were filtered out by excluding outliers in total counts, total features, and content of mitochondrial transcripts using Scater (*45*). Because the cells analyzed were sorted as $CD8^+$ cells, only cells expressing CD8A but not CD3, CD19, or AD79A were retained for analysis. Counts were normalized and scaled, variable features were detected, and dimensional reduction was performed using principal components analysis. Data from different patients were integrated using Harmony (*46*). Thereafter, neighbors were defined, all using Seurat's default parameters. Clusters were assigned using a resolution of 0.15. On the basis of the expression of activation markers IFN-γ, TNF, CD69, TNFRSF9, and PDCD1, we identified cluster 2 to be composed of activated cytotoxic T cells. TCR β chain sequences of single-cell RNA-seq were combined with TCR β chain sequences obtained from tumor-infiltrating lymphocytes. Common specificities were inferred using GLIPH2 (grouping of lymphocyte interactions by paratope hotspots 2) (*47*).

Statistics

Data were analyzed and graphed using GraphPad Prism (version 8, GraphPad Software Inc.). Statistical tests used are specified in the figure captions. The HRs and 95% CIs were obtained using the univariate Cox proportional hazards model in GraphPad Prism. Single-cell gene expression analysis was performed using Seurat version 4.0.4 (*44*). For details, please see the "Single-cell gene expression analysis" section.

Supplementary Materials

This PDF file includes:

Figs. S1 to S16

Tables S1 to S5, S7 and S8

Other Supplementary Material for this manuscript includes the following:

Tables S6 and S9

View/request a protocol for this paper from *Bio-protocol*.

REFERENCES AND NOTES

1. C. Robert, G. V. Long, B. Brady, C. Dutriaux, M. Maio, L. Mortier, J. C. Hassel, P. Rutkowski, C. McNeil, E. Kalinka-Warzocha, K. J. Savage, M. M. Hernberg, C. Lebbe, J. Charles, C. Mihalcioiu, V. Chiarion-Sileni, C. Mauch, F. Cognetti, A. Arance, H. Schmidt, D. Schadendorf, H. Gogas, L. Lundgren-Eriksson, C. Horak, B. Sharkey, I. M. Waxman, V. Atkinson, P. A. Ascierto, Nivolumab in previously untreated melanoma without BRAF mutation. *N. Engl. J. Med.* **372**, 320–330 (2015).
2. H. Borghaei, L. Paz-Ares, L. Horn, D. R. Spigel, M. Steins, N. E. Ready, L. Q. Chow, E. E. Vokes, E. Felip, E. Holgado, F. Barlesi, M. Kohlhaufl, O. Arrieta, M. A. Burgio, J. Fayette, H. Lena, E. Poddubskaya, D. E. Gerber, S. N. Gettinger, C. M. Rudin, N. Rizvi, L. Crino, G. R. Blumenschein Jr., S. J. Antonia, C. Dorange, C. T. Harbison, F. Graf Finckenstein, J. R. Brahmer, Nivolumab versus docetaxel in advanced nonsquamous non-small-cell lung cancer. *N. Engl. J. Med.* **373**, 1627–1639 (2015).
3. A. Rittmeyer, F. Barlesi, D. Waterkamp, K. Park, F. Ciardiello, J. von Pawel, S. M. Gadgeel, T. Hida, D. M. Kowalski, M. C. Dols, D. L. Cortinovis, J. Leach, J. Polikoff, C. Barrios, F. Kabbinavar, O. A. Frontera, F. De Marinis, H. Turna, J.-S. Lee, M. Ballinger, M. Kowanetz, P. He, D. S. Chen, A. Sandler, D. R. Gandara, Atezolizumab versus docetaxel in patients with previously treated non-small-cell lung cancer (OAK): A phase 3, open-label, multicentre randomised controlled trial. *Lancet* **389**, 255–265 (2017).
4. R. J. Motzer, B. Escudier, D. F. McDermott, S. George, H. J. Hammers, S. Srinivas, S. S. Tykodi, J. A. Sosman, G. Procopio, E. R. Plimack, D. Castellano, T. K. Choueiri, H. Gurney, F. Donskov, P. Bono, J. Wagstaff, T. C. Gauler, T. Ueda, Y. Tomita, F. A. Schutz, C. Kollmannsberger, J. Larkin, A. Ravaud, J. S. Simon, L. A. Xu, I. M. Waxman, P. Sharma, I. CheckMate, Nivolumab versus everolimus in advanced renal-cell carcinoma. *N. Engl. J. Med.* **373**, 1803–1813 (2015).
5. J. Bellmunt, R. de Wit, D. J. Vaughn, Y. Fradet, J. L. Lee, L. Fong, N. J. Vogelzang, M. A. Climent, D. P. Petrylak, T. K. Choueiri, A. Necchi, W. Gerritsen, H. Gurney, D. I. Quinn, S. Culine, C. N. Sternberg, Y. Mai, C. H. Poehlein, R. F. Perini, D. F. Bajorin; KEYNOTE-045, Pembrolizumab as second-line therapy for advanced urothelial carcinoma. *N. Engl. J. Med.* **376**, 1015–1026 (2017).
6. A. Bertrand, M. Kostine, T. Barnetche, M. E. Truchetet, T. Schaeverbeke, Immune related adverse events associated with anti-CTLA-4 antibodies: Systematic review and meta-analysis. *BMC Med.* **13**, 211 (2015).
7. Y. Wang, S. Zhou, F. Yang, X. Qi, X. Wang, X. Guan, C. Shen, N. Duma, J. Vera Aguilera, A. Chintakuntlawar, K. A. Price, J. R. Molina, L. C. Pagliaro, T. R. Halfdanarson, A. Grothey, S. N. Markovic, G. S. Nowakowski, S. M. Ansell, M. L. Wang, Treatment-related adverse events of PD-1 and PD-L1 inhibitors in clinical trials: A systematic review and meta-analysis. *JAMA Oncol.* **5**, 1008–1019 (2019).
8. J. R. Brahmer, C. Lacchetti, B. J. Schneider, M. B. Atkins, K. J. Brassil, J. M. Caterino, I. Chau, M. S. Ernstoff, J. M. Gardner, P. Ginex, S. Hallmeyer, J. H. Chakrabarty, N. B. Leighl, J. S. Mammen, D. F. McDermott, A. Naing, L. J. Nastoupil, T. Phillips, L. D. Porter, I. Puzanov, C. A. Reichner, B. D. Santomasso, C. Seigel, A. Spira, M. E. Suarez-Almazor, Y. Wang, J. S. Weber, J. D. Wolchok, J. A. Thompson; National Comprehensive Cancer Network, Management of immune-related adverse events in patients treated with immune checkpoint inhibitor therapy: American society of clinical oncology clinical practice guideline. *J. Clin. Oncol.* **36**, 1714–1768 (2018).
9. F. Petrelli, G. Grizzi, M. Ghidini, A. Ghidini, M. Ratti, S. Panni, M. Cabiddu, M. Ghilardi, K. Borgonovo, M. C. Parati, G. Tomasello, S. Barni, A. Berruti, M. Brighenti, Immune-related adverse events and survival in solid tumors treated with immune checkpoint inhibitors: A systematic review and meta-analysis. *J. Immunother.* **43**, 1–7 (2020).
10. C. Nardin, A. Jeand'heur, K. Bouiller, M. B. Valnet-Rabier, F. Dresco, J. Castagna, A. Mareschal, C. Carlet, V. Nerich, S. Limat, E. Puzenat, F. Aubin, Vitiligo under anti-programmed cell death-1 therapy is associated with increased survival in melanoma patients. *J. Am. Acad. Dermatol.* **82**, 770–772 (2020).
11. B. Palermo, R. Campanelli, S. Garbelli, S. Mantovani, E. Lantelme, V. Brazzelli, M. Ardigo, G. Borroni, M. Martinetti, C. Badulli, A. Necker, C. Giachino, Specific cytotoxic T lymphocyte responses against Melan-A/MART1, tyrosinase and gp100 in vitiligo by the use of major histocompatibility complex/peptide tetramers: The role of cellular immunity in the etiopathogenesis of vitiligo. *J. Invest. Dermatol.* **117**, 326–332 (2001).
12. M. Nishino, A. Giobbie-Hurder, H. Hatabu, N. H. Ramaiya, F. S. Hodi, Incidence of programmed cell death 1 inhibitor-related pneumonitis in patients with advanced cancer: A systematic review and meta-analysis. *JAMA Oncol.* **2**, 1607–1616 (2016).
13. A. Bate, S. J. Evans, Quantitative signal detection using spontaneous ADR reporting. *Pharmacoepidemiol. Drug Saf.* **18**, 427–436 (2009).
14. The Cancer Genome Atlas Research Network, Comprehensive genomic characterization of squamous cell lung cancers. *Nature* **489**, 519–525 (2012).
15. P. Reemann, E. Reimann, S. Ilmjarv, O. Porosaar, H. Silm, V. Jaks, E. Vasar, K. Kingo, S. Koks, Melanocytes in the skin--comparative whole transcriptome analysis of main skin cell types. *PLOS ONE* **9**, e115717 (2014).
16. J. Pitcovski, E. Shahar, E. Aizenshtein, R. Gorodetsky, Melanoma antigens and related immunological markers. *Crit. Rev. Oncol. Hematol.* **115**, 36–49 (2017).
17. J. Park, A. H. Talukder, S. A. Lim, K. Kim, K. Pan, B. Melendez, S. D. Bradley, K. R. Jackson, J. S. Khalili, J. Wang, C. Creasy, B. F. Pan, S. E. Woodman, C. Bernatchez, D. Hawke, P. Hwu, K. M. Lee, J. Roszik, G. Lizee, C. Yee, SLC45A2: A melanoma antigen with high tumor selectivity and reduced potential for autoimmune toxicity. *Cancer Immunol. Res.* **5**, 618–629 (2017).
18. B. M. Turner, P. T. Cagle, I. M. Sainz, J. Fukuoka, S. S. Shen, J. Jagirdar, Napsin A, a new marker for lung adenocarcinoma, is complementary and more sensitive and specific than thyroid transcription factor 1 in the differential diagnosis of primary pulmonary carcinoma: Evaluation of 1674 cases by tissue microarray. *Arch. Pathol. Lab. Med.* **136**, 163–171 (2012).
19. S. Song, M. Han, H. Zhang, Y. Wang, H. Jiang, Full screening and accurate subtyping of HLA-A*02 alleles through group-specific amplification and mono-allelic sequencing. *Cell. Mol. Immunol.* **10**, 490–496 (2013).
20. S. C. Weinmann, D. S. Pisetsky, Mechanisms of immune-related adverse events during the treatment of cancer with immune checkpoint inhibitors. *Rheumatology (Oxford)* **58**, vii59–vii67 (2019).
21. T. Matsuda, M. Leisegang, J. H. Park, L. Ren, T. Kato, Y. Ikeda, M. Harada, K. Kiyotani, E. Lengyel, G. F. Fleming, Y. Nakamura, Induction of neoantigen-specific cytotoxic t cells and construction of T-cell receptor-engineered t cells for ovarian cancer. *Clin. Cancer Res.* **24**, 5357–5367 (2018).
22. F. Berner, D. Bomze, S. Diem, O. H. Ali, M. Fassler, S. Ring, R. Niederer, C. J. Ackermann, P. Baumgaertner, N. Pikor, C. G. Cruz, W. van de Veen, M. Akdis, S. Nikolaev, H. Laubli, A. Zippelius, F. Hartmann, H. W. Cheng, G. Honger, M. Recher, J. Goldman, A. Cozzio, M. Fruh, J. Neefjes, C. Driessen, B. Ludewig, A. N. Hegazy, W. Jochum, D. E. Speiser, L. Flatz, Association of checkpoint inhibitor-induced toxic effects with shared cancer and tissue antigens in non-small cell lung cancer. *JAMA Oncol.* **5**, 1043–1047 (2019).
23. J. A. Lo, M. Kawakubo, V. R. Juneja, M. Y. Su, T. H. Erlich, M. W. LaFleur, L. V. Kemeny, M. Rashid, M. Malehmir, S. A. Rabi, R. Raghavan, J. Allouche, G. Kasumova, D. T. Frederick, K. E. Pauken, Q. Y. Weng, M. P. da Silva, Y. Xu, A. A. J. van der Sande, W. Silkworth, E. Roider, E. P. Browne, D. J. Lieb, B. Wang, L. A. Garraway, C. J. Wu, K. T. Flaherty, C. E. Brinckerhoff, D. W. Mullins, D. J. Adams, N. Hacohen, M. P. Hoang, G. M. Boland, G. J. Freeman, A. H. Sharpe, D. Manstein, D. E. Fisher, Epitope spreading toward wild-type melanocyte-lineage antigens rescues suboptimal immune checkpoint blockade responses. *Sci. Transl. Med.* **13**, eabd8636 (2021).
24. E. Braunlein, A. M. Krackhardt, Tools to define the melanoma-associated immunopeptidome. *Immunology* **152**, 536–544 (2017).
25. T. Bilich, A. Nelde, L. Bichmann, M. Roerden, H. R. Salih, D. J. Kowalewski, H. Schuster, C. C. Tsou, A. Marcu, M. C. Neidert, M. Lübke, J. Rieth, M. Schemionek, T. H. Brümmendorf, V. Vucinic, D. Niederwieser, J. Bauer, M. Märklin, J. K. Peper, R. Klein, O. Kohlbacher, L. Kanz, H. G. Rammensee, S. Stevanovic, J. S. Walz, The HLA ligandome landscape of chronic myeloid leukemia delineates novel T-cell epitopes for immunotherapy. *Blood* **133**, 550–565 (2019).
26. K. Yasumoto, T. Hanagiri, M. Takenoyama, Lung cancer-associated tumor antigens and the present status of immunotherapy against non-small-cell lung cancer. *Gen. Thorac. Cardiovasc. Surg.* **57**, 449–457 (2009).
27. K. Esfahani, A. Elkrief, C. Calabrese, R. Lapointe, M. Hudson, B. Routy, W. H. Miller Jr., L. Calabrese, Moving towards personalized treatments of immune-related adverse events. *Nat. Rev. Clin. Oncol.* **17**, 504–515 (2020).
28. A. Marcu, L. Bichmann, L. Kuchenbecker, D. J. Kowalewski, L. K. Freudenmann, L. Backert, L. Muhlenbruch, A. Szolek, M. Lubke, P. Wagner, T. Engler, S. Matovina, J. Wang, M. Hauri-Hohl, R. Martin, K. Kapolou, J. S. Walz, J. Velz, H. Moch, L. Regli, M. Silginer, M. Weller, M. W. Loffler, F. Erhard, A. Schlosser, O. Kohlbacher, S. Stevanovic, H. G. Rammensee, M. C. Neidert, HLA ligand atlas: A benign reference of HLA-presented peptides to improve T-cell-based cancer immunotherapy. *J. Immunother. Cancer* **9**, e002071 (2021).
29. P. J. Thul, C. Lindskog, The Human Protein Atlas: A spatial map of the human proteome. *Protein Sci.* **27**, 233–244 (2018).
30. K. Yasumoto, K. Yokoyama, K. Shibata, Y. Tomita, S. Shibahara, Microphthalmia-associated transcription factor as a regulator for melanocyte-specific transcription of the human tyrosinase gene. *Mol. Cell. Biol.* **14**, 8058–8070 (1994).
31. S. Hänzelmann, R. Castelo, J. Guinney, GSVA: Gene set variation analysis for microarray and RNA-Seq data. *BMC Bioinformatics* **14**, 7 (2013).
32. A. Nelde, D. J. Kowalewski, S. Stevanovic, Purification and identification of naturally presented MHC class I and II ligands. *Methods Mol. Biol.* **1988**, 123–136 (2019).
33. D. J. Kowalewski, H. Schuster, L. Backert, C. Berlin, S. Kahn, L. Kanz, H. R. Salih, H. G. Rammensee, S. Stevanovic, J. Sarah Stickel, HLA ligandome analysis identifies the

underlying specificities of spontaneous antileukemia immune responses in chronic lymphocytic leukemia (CLL). *Proc. Natl. Acad. Sci. U.S.A.* **112**, E166–E1675 (2015).
34. E. Milner, L. Gutter-Kapon, M. Bassani-Strenberg, E. Barnea, I. Beer, A. Admon, The effect of proteasome inhibition on the generation of the human leukocyte antigen (HLA) peptidome. *Mol. Cell. Proteomics* **12**, 1853–1864 (2013).
35. L. Käll, J. D. Canterbury, J. Weston, W. S. Noble, M. J. MacCoss, Semi-supervised learning for peptide identification from shotgun proteomics datasets. *Nat. Methods* **4**, 923–925 (2007).
36. M. M. Schuler, M. D. Nastke, S. Stevanovic, SYFPEITHI: Database for searching and T-cell epitope prediction. *Methods Mol. Biol.* **409**, 75–93 (2007).
37. V. Jurtz, S. Paul, M. Andreatta, P. Marcatili, B. Peters, M. Nielsen, NetMHCpan-4.0: Improved peptide-MHC class I interaction predictions integrating eluted ligand and peptide binding affinity data. *J. Immunol.* **199**, 3360–3368 (2017).
38. J. J. Luimstra, K. Franken, M. A. Garstka, J. W. Drijfhout, J. Neefjes, H. Ovaa, Production and thermal exchange of conditional peptide-MHC I multimers. *Curr. Protoc. Immunol.* **126**, e85 (2019).
39. J. J. Luimstra, M. A. Garstka, M. C. J. Roex, A. Redeker, G. M. C. Janssen, P. A. van Veelen, R. Arens, J. H. F. Falkenburg, J. Neefjes, H. Ovaa, A flexible MHC class I multimer loading system for large-scale detection of antigen-specific T cells. *J. Exp. Med.* **215**, 1493–1504 (2018).
40. A. Reuben, J. Zhang, S. H. Chiou, R. M. Gittelman, J. Li, W. C. Lee, J. Fujimoto, C. Behrens, X. Liu, F. Wang, K. Quek, C. Wang, F. Kheradmand, R. Chen, C. W. Chow, H. Lin, C. Bernatchez, A. Jalali, X. Hu, C. J. Wu, A. K. Eterovic, E. R. Parra, E. Yusko, R. Emerson, S. Benzeno, M. Vignali, X. Wu, Y. Ye, L. D. Little, C. Gumbs, X. Mao, X. Song, S. Tippen, R. L. Thornton, T. Cascone, A. Snyder, J. A. Wargo, R. Herbst, S. Swisher, H. Kadara, C. Moran, N. Kalhor, J. Zhang, P. Scheet, A. A. Vaporciyan, B. Sepesi, D. L. Gibbons, H. Robins, P. Hwu, J. V. Heymach, P. Sharma, J. P. Allison, V. Baladandayuthapani, J. J. Lee, M. M. Davis, I. I. Wistuba, P. A. Futreal, J. Zhang, Comprehensive T cell repertoire characterization of non-small cell lung cancer. *Nat. Commun.* **11**, 603 (2020).
41. J. Kargl, S. E. Busch, G. H. Yang, K. H. Kim, M. L. Hanke, H. E. Metz, J. J. Hubbard, S. M. Lee, D. K. Madtes, M. W. McIntosh, A. M. Houghton, Neutrophils dominate the immune cell composition in non-small cell lung cancer. *Nat. Commun.* **8**, 14381 (2017).
42. S. Valpione, E. Galvani, J. Tweedy, P. A. Mundra, A. Banyard, P. Middlehurst, J. Barry, S. Mills, Z. Salih, J. Weightman, A. Gupta, G. Gremel, F. Baenke, N. Dhomen, P. C. Lorigan, R. Marais, Immune-awakening revealed by peripheral T cell dynamics after one cycle of immunotherapy. *Nat. Cancer* **1**, 210–221 (2020).
43. W. Pruessmann, J. Rytlewski, J. Wilmott, M. C. Mihm Jr., G. H. Attrill, B. Dyring-Andersen, P. Fields, Q. Zhan, A. J. Colebatch, P. M. Ferguson, J. F. Thompson, K. Kallenbach, E. Yusko, R. A. Clark, H. Robins, R. A. Scolyer, T. S. Kupper, Molecular analysis of primary melanoma T cells identifies patients at risk for metastatic recurrence. *Nat. Cancer* **1**, 197–209 (2020).
44. Y. Hao, S. Hao, E. Andersen-Nissen, W. M. Mauck III, S. Zheng, A. Butler, M. J. Lee, A. J. Wilk, C. Darby, M. Zager, P. Hoffman, M. Stoeckius, E. Papalexi, E. P. Mimitou, J. Jain, A. Srivastava, T. Stuart, L. M. Fleming, B. Yeung, A. J. Rogers, J. M. McElrath, C. A. Blish, R. Gottardo, P. Smibert, R. Satija, Integrated analysis of multimodal single-cell data. *Cell* **184**, 3573–3587.e29 (2021).
45. D. J. McCarthy, K. R. Campbell, A. T. Lun, Q. F. Wills, Scater: Pre-processing, quality control, normalization and visualization of single-cell RNA-seq data in R. *Bioinformatics* **33**, 1179–1186 (2017).
46. I. Korsunsky, N. Millard, J. Fan, K. Slowikowski, F. Zhang, K. Wei, Y. Baglaenko, M. Brenner, P. R. Loh, S. Raychaudhuri, Fast, sensitive and accurate integration of single-cell data with Harmony. *Nat. Methods* **16**, 1289–1296 (2019).
47. H. Huang, C. Wang, F. Rubelt, T. J. Scriba, M. M. Davis, Analyzing the *Mycobacterium tuberculosis* immune response by T-cell receptor clustering with GLIPH2 and genome-wide antigen screening. *Nat. Biotechnol.* **38**, 1194–1202 (2020).

Acknowledgments: We thank L. Robinson from Insight Editing London for critical review and editing of the manuscript. We thank BioRender for providing us with images that allowed us to create Fig. 5. **Funding:** This project received funding from the Swiss National Science Foundation (PP00P3_157448), Swiss Cancer League (KLS-4409-02-2018), the Forschungsförderung of the Kantonsspital St. Gallen, Hookipa Pharma, and Novartis Foundation. L.F. discloses advisory roles for Novartis, Sanofi, and Bristol-Myers Squibb. O.H.A. is supported by a Swiss National Science Foundation grant (PMP400PM_194473). **Author contributions:** F.B., D.B., J.W., and L.F. contributed to experimental design. F.B., D.B., C.L., A.-K.J., J.B., L.K.F., A.M., E.-M.W., S.H., T.G., T.S., K.H., H.L., M.-T.A., R.N., S.K., S.P., J.N., H.-G.R., M.H., N.K., M.T., N.W., V.W.. and H.-W.C. contributed to data acquisition. F.B., D.B., J.B., V.W., J.W., and L.F. contributed to data interpretation and analysis. F.B., R.N., M.-T.P., C.L., O.T.P., A.-K.J., W.J., S.D., M.J., M.F., O.H.A., and L.F. contributed to sample and patient data collection and processing. F.B., D.B., L.F., J.W., and J.N. contributed to writing and/or critically revising the manuscript for important intellectual content. M.-T.A. provided technical support. L.F. was responsible for funding and study supervision. **Competing interests:** L.K.F. is a current employee of Immatics Biotechnologies. The other authors declare that they have no competing interests. **Data and materials availability:** Single-cell RNA-seq datasets have been deposited in Zenodo (6884319). TCR sequencing datasets have been deposited in the Adaptive Biotechnologies immuneACCESS platform (10.21417/FB2022SI, available at clients.adaptivebiotech.com/pub/berner-2022-si). All data needed to evaluate the conclusions in the paper are present in the paper or the Supplementary Materials.

Submitted 4 January 2022
Accepted 10 August 2022
Published 2 September 2022
10.1126/sciimmunol.abn9644

Science Immunology

Autoreactive napsin A–specific T cells are enriched in lung tumors and inflammatory lung lesions during immune checkpoint blockade

Fiamma Berner, David Bomze, Christa Lichtensteiger, Vincent Walter, Rebekka Niederer, Omar Hasan Ali, Nina Wyss, Jens Bauer, Lena Katharina Freudenmann, Ana Marcu, Eva-Maria Wolfschmitt, Sebastian Haen, Thorben Gross, Marie-Therese Abdou, Stefan Diem, Stella Knpfli, Tobias Sinnberg, Kathrin Hofmeister, Hung-Wei Cheng, Marieta Toma, Niklas Klmper, Mette-Triin Purde, Oltin Tiberiu Pop, Ann-Kristin Jochum, Steve Pascolo, Markus Joerger, Martin Frh, Wolfram Jochum, Hans-Georg Rammensee, Heinz Lubli, Michael Hlzel, Jacques Neefjes, Juliane Walz, and Lukas Flatz

Sci. Immunol., **7** (75), eabn9644.
DOI: 10.1126/sciimmunol.abn9644

irAE causing T cells in lung cancer

Despite the success of immune checkpoint blockade (ICB) in cancer, the efficacy is limited by immune-related adverse events (irAEs) that require treatment cessation. Thus, identifying peptides that induce both antitumor and irAE responses is crucial to improving ICB. Here, Berner *et al.* developed a method, DITAS (discovery of tumor-associated self-antigens) for detecting these peptides. DITAS involved analyzing the shared antigens between non–small cell lung cancer (NSCLC) and lung tissue, then performing immunopeptidomes, determining which HLA these peptides bound to, predicting the CD8+ T cell epitopes of these peptides, performing functional validation, and lastly identifying their candidate antigens. Using this method, the authors identified napsin A, which induced NSCLC and lung reactive T cells. Thus, DITAS could be used to identify irAE causing T cells.

Science Immunology (ISSN) is published by the American Association for the Advancement of Science. 1200 New York Avenue NW, Washington, DC 20005. The title *Science Immunology* is a registered trademark of AAAS.